1st International Conference on Experiments/Process/System Modelling/Simulation/Optimization
1st IC-EpsMsO
Athens, 6-9 July, 2005

IMAGE-BASED COMPUTATIONAL FLUID DYNAMICS AND STRUCTURAL ANALYSIS IN ABDOMINAL AORTIC ANEURYSMS

Yannis Papaharilaou [*,♣], John A. Ekaterinaris[*], Eirini Manousaki[♣], Asterios N. Katsamouris[♣]

[*]Institute of Applied and Computational Mathematics
Foundation for Research and Technology- Hellas
P.O.BOX 1527, 71110 Heraklion, Crete, Greece
e-mail: yannisp@iacm.forth.gr, web page: http://www.iacm.forth.gr

[♣] Dept. of Vascular Surgery, University of Crete, Greece

Keywords: Biofluid mechanics, aneurysm rupture, computational hemodynamics, structural stress analysis.

Abstract. *Abdominal aortic aneurysm (AAA) is a localized dilatation of the aortic wall. The lack of an accurate AAA rupture risk index remains an important problem in the clinical management of the disease. To accurately estimate AAA rupture risk, detailed information on patient specific wall stress distribution and aortic wall tissue yield stress is required. A complete fluid structure interaction (FSI) study of the wall forces is impractical and thus of limited clinical value. On the other hand, isolated static structural stress analysis based on a uniform wall loading is a widely used approach for AAA rupture risk estimation that however neglects flow induced wall stress variation. Aim of this study was to assess the merit of a decoupled fluid structure analysis of AAA wall stress. Anatomically correct patient specific AAA wall models were created by 3D reconstruction of computed tomography (CT) images. Flow simulations were carried out with inflow and outflow boundary conditions obtained from patient extracted data. Static structural stress analysis was performed applying a uniform pressure wall loading and a flow induced non-uniform pressure loading. In the structural analysis a hyperelastic arterial wall model and an elastic intraluminal thrombus (ILT) model were applied. Our results show that the decoupled fluid structural analysis approach yields a more realistic AAA wall stress distribution than the isolated structural stress analysis approach thus providing a practical alternative to the more complete but computationally intensive FSI study.*

1 INTRODUCTION

Abdominal aortic aneurysm is a localized dilatation of the aortic wall. The physiological processes associated with AAA development and progression are not yet fully understood. This pathologic condition has been found to affect 8.8 % of the population over the age of 65 [1] and if left untreated it may lead to rupture. The size of the aneurysm and its rate of expansion are parameters associated with the risk of rupture. The risk of rupture for aneurysms with a maximum transverse diameter below 4 cm is very small (but not absent). However, when the aneurysm transverse diameter is between 4 and 5 cm the risk of rupture is 0.5 % and between 5 and 6 cm it becomes 5 % rising exponentially with diameter increase [2-4]. The decision for surgical intervention for patients with AAA's is complicated by the lack of a sufficiently accurate rupture risk index. A widely used such index, based on the results from a number of studies [5-7], is the maximum transverse diameter. In cases where this diameter exceeds 5-6 cm, surgical or endovascular treatment is advised. However 'small' (<5 cm) diameter aneurysms, where 'watchful waiting' requiring frequent observation is preferred to surgery, are known to rupture [8-10]. Therefore, the decision for surgical intervention, associated with a mortality rate of 4-5 % [11], should not be based exclusively on the maximum transverse diameter and a new more reliable rupture risk index should be introduced.

Finite element analysis (FEA) has been used to compute the stress distribution in both simplified [12,13] and anatomically correct [14,15] AAA models. The hemodynamics of the AAA have been extensively investigated experimentally [16,17] and computationally in both idealized and anatomically correct models in steady and time varying flow [18,19]. The coupling of fluid and structure has also been studied in AAA models [20]. The role of ILT on AAA wall stress still remains uncertain. Some studies support the hypothesis that the ILT introduces a cushioning effect in the transmission of the flow induced stresses to the wall that reduces the peak wall stress [21-23], while others suggest that thrombus has no effect on the progression of an AAA [24,25]. Various simplifications have been introduced to the models used in these studies with respect to the shape of the aneurysm, the inclusion and elastic properties of ILT, the thickness and elastic properties of the wall, the role of surrounding structures and, the presence of residual stresses on the AAA wall.

The stress distribution on the aneurysmal wall is determined by the complex intra-aneurysmal hemodynamics resulting from the complex geometric configuration of the ILT modulated flow conduit. The maximum transverse dimension of the AAA is being used routinely in clinical practice as an estimate of rupture risk. However, the use of this parameter alone has lead in many cases to the underestimation of rupture risk in 'small' (<5 cm) diameter aneurysms and overestimation of the risk of rupture in 'large' (>6 cm) diameter aneurysms thus compromising the quality of patient management.

The lack of an accurate AAA rupture risk index remains an important problem in the clinical management of the disease. Accurate estimation of the patient specific AAA rupture risk requires detailed information on both the wall stress distribution and the aortic wall tissue yield stress. However, the AAA wall properties and the stress distribution cannot be measured or even derived with sufficient accuracy from non-invasive measurements *in vivo*. As an alternative, numerical approximations of the flow and wall motion equations are sought using wall constitutive models based on mean elastic properties obtained by mechanical testing of excised specimens of the aneurismal wall. Rhagavan et al. [26] proposed a two parameter, hyperelastic, isotropic, incompressible material model for the AAA wall utilizing uniaxial loading stress strain measurements on excised AAA specimens. The ILT solid structure has been modeled as either an elastic [27] or hyperelastic [28], isotropic, incompressible material.

The wall stress computation should ideally result from a complete FSI simulation of the wall forces. However, this approach is very intensive computationally and thus currently impractical. Furthermore, it has been shown in idealized AAA models that the FSI approach yields peak wall stress estimates similar to those obtained by an *isolated* structural stress analysis [29]. The computational approach most widely used to estimate peak AAA wall stress is the isolated static structural analysis with a uniform peak systolic pressure wall loading. However, this approach neglects the flow induced pressure distribution on the AAA wall. Aim of this study was to assess the merit of a decoupled fluid structure approach for AAA wall stress estimation as compared to the isolated static structural stress analysis approach. Towards this end the stress distribution computed for a uniform wall loading in an anatomically correct AAA model is compared to the stress computed for the same model but for the flow induced pressure wall loading.

2 METHODS

A 86 year old male with an intact 10 cm peak transverse diameter AAA was the subject selected for this study. The selected aneurysm geomerty exhibits significant tortouosity of the inflow conduit and the proximal segments of the iliac arteries that is expected to strongly affect the intraaneurysmal flow field. This geometric configuration is typical of large AAA's and can be attributed to the asymmetric expansion of the aneurysm sac caused primarily by the expansion direction restricitons introduced by the proximity of the spinal column. Information on the 3D AAA geometric configuration was extracted *in vivo* by contrast enhanced high resolution spiral CT angiography. The CT acquisition parameters were prescribed: 160 mAs, 120 kVp, 10.4 s scan time, 22.1 mm feed/rotation ratio, 380 mm in plane FOV, 2 mm slice thickness, 1.5 mm reconstruction spacing/increment, 0.5 mm slice overlap and a 512 x 512 image matrix size resulting in a 0.742 mm in plane resolution. Angiography was triggered at 120 Houndsfield units.

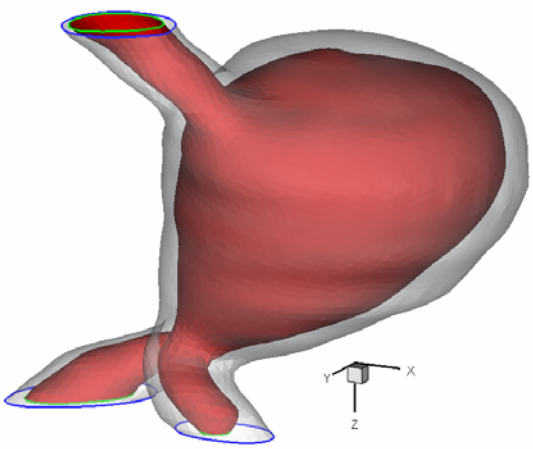

Figure 1. Internal (red) and external (grey-translucent) 3D reconstructed smoothed surfaces of the CT image extracted AAA geometry.

Segmentation and 3D surface reconstruction of the CT images was implemented using in house developed software [30]. From the segmented CT images two 3D surfaces were reconstructed: the true vessel lumen surface

and the external aortic wall surface (Figure 1). A third surface, the internal aortic wall was generated as an iso-surface 2 mm inwards from the external aortic wall. The third surface, the interface between the AAA wall endothelium and the ILT, could not be extracted from the CT images as the imaging method still lacks the level of spatial resolution and contrast required. The location of this third surface relative to the external aortic wall surface effectively determines the thickness of the AAA wall. Abnormal, small scale surface irregularities introduced during the imaging and reconstruction processes were excluded from the computational model by applying pixel width constrained smoothing of the reconstructed surfaces prior to mesh generation.

2.1 Flow Computation

The computational grid generated using Gambit had 333150 tetrahedral elements and non-uniform grid node spacing to produce higher grid density at the proximal and distal aneurysm neck regions as compared to the bulge surface. A short, native vessel blended straight tube like extension of the proximal inflow was added to the model to create a circular cross section inlet required for the correct application of the exact Womersley solution as the time dependent inflow boundary condition. The Navier-Stokes and continuity equations for incompressible flow neglecting body forces are expressed in vector form as:

$$\nabla \cdot \mathbf{u} = 0$$

$$\frac{D\mathbf{u}}{Dt} = -\frac{1}{\rho}\nabla p + \nu\nabla^2\mathbf{u}$$

where, $D/Dt = \partial/\partial t + \mathbf{u}\cdot\nabla$ is the substantial derivative, ρ is the fluid density, and v is the fluid kinematic viscosity.

Fluent 6.1.22 was used to solve the flow equations. For the flow field computations, the arterial wall was assumed rigid and blood was modeled as an incompressible, Newtonian fluid with a density of 1.05 gr/cm^3 and a viscosity of 4.5 cP. Blood is a suspension of red and white cells, platelets, proteins and other elements in plasma and exhibits an anomalous non Newtonian viscous behavior when exposed to low shear rates or flows in tubes of less than 1mm in diameter. However, the Newtonian fluid assumption does not affect the major flow features and is considered acceptable for modeling blood flow in the macrocirculation [31]. The AAA inflow waveform and the aortic flow split ratio in the iliac arteries were measured *in vivo* by Doppler US two hours after CT scanning of the patient. On average the left iliac artery received 40 % of the aortic flow and the right iliac artery received 60 %. The discrete Fourier series of the measured AAA inflow waveform can be expressed as:

$$Q(t) = Q_0 + \sum_{n=1}^{N} Q_n e^{in\omega t}$$

where Q_0 is the steady flow component, N=16 represents the number of Fourier modes used and ω is the fundamental frequency of the measured flow waveform. From the discrete Fourier series the fully developed time varying velocity profile applied at the model inlet was computed using an expression obtained following Womersley's derivation [32]:

$$u(r,t) = \frac{2Q_0}{A}\left(1-\frac{r^2}{R^2}\right) + \sum_{n=1}^{N}\frac{Q_n}{A}\left\{\left(1-\frac{J_0(\alpha_n i^{3/2} r/R)}{J_0(\alpha_n i^{3/2})}\right)/\left(1-\frac{2J_1(\alpha_n i^{3/2})}{\alpha_n i^{3/2} J_0(\alpha_n i^{3/2})}\right)\right\} e^{in\omega t}$$

where J_0 and J_1 are the Bessel functions of the first kind of order zero and one respectively, A is the cross sectional area and R the inlet radius of the straight tube extension inlet and, $\alpha_n = R\sqrt{n\omega/\nu}$ is the Womersley parameter. The time averaged mean Reynolds number of the prescribed waveform was Re_m=355 and the Womersley parameter for the fundamental frequency of the measured flow waveform was α_1=16.7. A time step size of 6×10^{-4} s was used and 10^4 time steps were required to complete one flow cycle. A time periodic solution was achieved after 7 flow cycles. A second order upwind discretization scheme was applied for the momentum equation and the SIMPLE scheme was used for pressure velocity coupling.

2.2 Finite element stress analysis

ABAQUS 6.4.1 was used to solve the momentum equations, the wall constitutive equations and the conditions of equilibrium for the static structural stress analysis. The aortic wall was modeled as an incompressible, homogenous, isotropic, hyperelastic, material with a uniform thickness of 2 mm. The finite strain constitutive model proposed by Rhagavan et al. [26] was adopted for the arterial wall with a strain energy density function given by

$$W = \alpha(I_B - 3) + \beta(I_B - 3)^2$$

where, I_B is the first invariant of the left Cauchy-Green tensor **B** (I_B=tr **B**). The model parameters were set to α= 17.4 N cm^{-2} and β =188.1 N cm^{-2} that correspond to population mean values obtained from uniaxial loading tests on excised AAA wall specimens.

The ILT was modeled as an incompressible, isotropic, homogenous, linear elastic material with a Young modulus E = 0.11 MPa and a Poisson ratio ν = 0.45. These values of E and ν represent population mean values obtained from uniaxial loading tests performed on ILT specimens harvested during AAA surgery by Di Martino et al. [27]. The AAA model assembly included the ILT solid part with 41291 tetrahedral elements and the arterial wall shell part with 9690 triangular elements. Stress analysis results were obtained both for a uniform wall loading using the peak systolic arterial pressure (16 kPa or 120 mmHg) and for the non-uniform flow induced wall pressure loading computed during early systolic deceleration. Mapping of the pressure field from the fine numerical grid required for the flow computations to the coarser grid used in the stress analysis was achieved by inverse-distance interpolation. A non-slip condition was applied at the AAA wall - ILT interface. The proximal and distal ends of the model were constrained longitudinally.

3 RESULTS

The results of the time dependent flow field computation showed that most of the AAA lumen wall surface was exposed to very low wall shear stress (WSS) throughout the cardiac cycle. Regions of locally elevated WSS were located near the proximal and distal neck of the AAA bulge (Figure 2a). WSS magnitude was normalized by the straight pipe inlet Poiseuille WSS. The computed wall pressure distribution during early systolic deceleration (Figure 2b) showed a significant deviation from the peak arterial systolic pressure which has been widely used as a uniform wall loading condition in static structural stress analyses. During early systolic acceleration regions in the vicinity of the distal neck of the aneurysmal wall were exposed to a pressure loading 18 % higher than the peak systolic pressure. Furthermore, most of the aneurysm bulge wall was exposed to pressures 10 % higher than the peak systolic pressure.

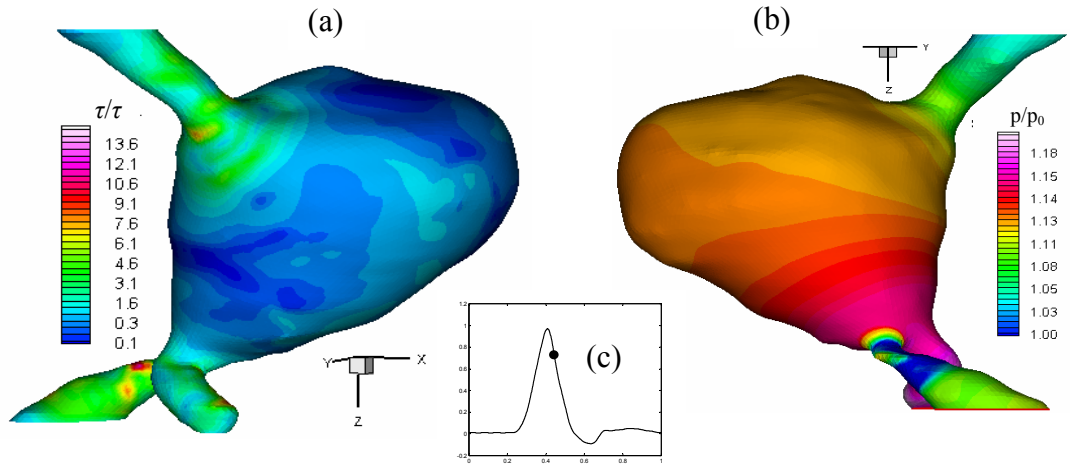

Figure 2. Computed WSS magnitude (a) and static pressure on the wall of the true lumen (b) during early systolic deceleration. WSS is normalized by the inlet equidiameter straight pipe WSS and static pressure is normalized by the systolic arterial pressure. The aortic flow waveform applied is also shown (c).

The highly complex flow field that develops in the aneurysmal sac is depicted in Figure 3 by means of stream ribbons color mapped with static pressure (a) and vorticity magnitude (b). The out of plane curvature (tortuosity) of the aortic flow conduit injecting blood into the aneurysmal expansion strongly influences the velocity distribution at the aneurismal bulge inlet. The vorticity colour mapped stream ribbon graph (Figure 3b) clearly depicts the increase in vorticity occurring within the tortuous aortic segment leading to the aneurysmal bulge inlet.

To obtain an estimate of particle residence time in the complex aneurysmal flow domain, massless particles were periodically released from a surface near the AAA model inlet (Fig. 4) and tracked for 10 flow cycles. The first particle exited the flow domain approximately after 5 cycles (Fig 4a). For the same inflow conditions the mean time required by a particle to flow through a straight pipe of the same length was found to be approximately 3 times less. This is partly explained by the strong recirculation regions associated with the rapid expansion of the aortic wall at the proximal neck and the adverse pressure gradient that develops which decelerates the particles and increases the mean particle path length. Snapshots of particle distribution during the

systolic deceleration phase are shown both after 5 cycles (Fig 4a) and during the last cycle (Fig. 4b). When particles were tracked for 35 cycles, it was found that a fraction of the particles released during the first flow cycle still remained trapped in the aneurysmal sac even after 35 cycles.

Stress distributions on the wall are presented using the Von-Mises stress, a scalar measure of the stress tensor that is proportional to the strain energy density at each point expressed as

$$\sigma_{VM} = \sqrt{\frac{1}{2}\left[(\sigma_1 - \sigma_2)^2 + (\sigma_1 - \sigma_3)^2 + (\sigma_2 - \sigma_3)^2\right]}$$

where σ_1, σ_2, σ_3 are the principal stresses. Application of the non-uniform flow induced wall loading to the AAA model produced a 12 % increase in the computed peak wall stress as compared to the uniform wall loading result (Figures 5 and 6). Two regions of high stress were found, one located anteriorly in the distal half of the AAA bulge with a local peak of 52 N/cm^2 (Figure 5 arrow) and the other located at the proximal neck anteriorly and to the left with a local peak of 54 N/cm^2 (Figure 6 arrow). It should be noted that only the magnitude and not the locations of the peak stress regions was altered by the introduction of the non-uniform flow induced pressure wall loading.

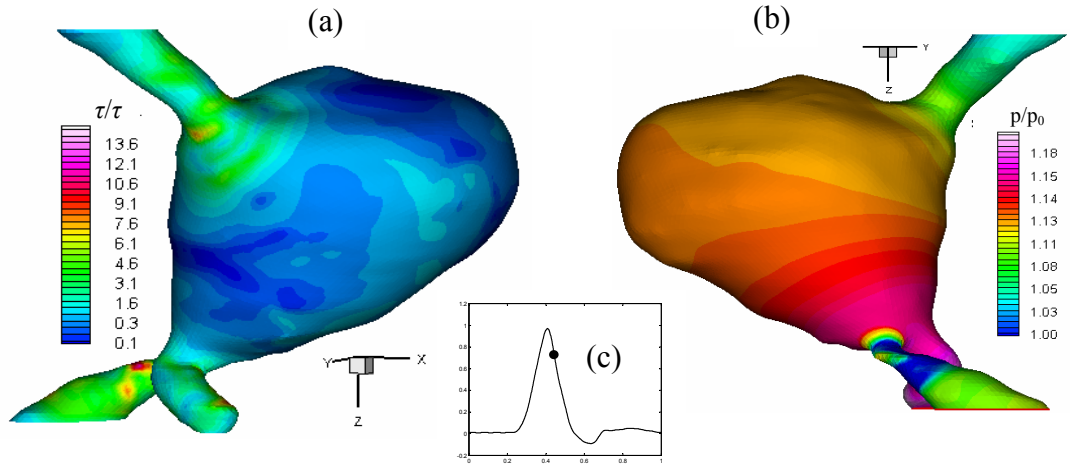

Figure 2. Computed WSS magnitude (a) and static pressure on the wall of the true lumen (b) during early systolic deceleration. WSS is normalized by the inlet equidiameter straight pipe WSS and static pressure is normalized by the systolic arterial pressure. The aortic flow waveform applied is also shown (c).

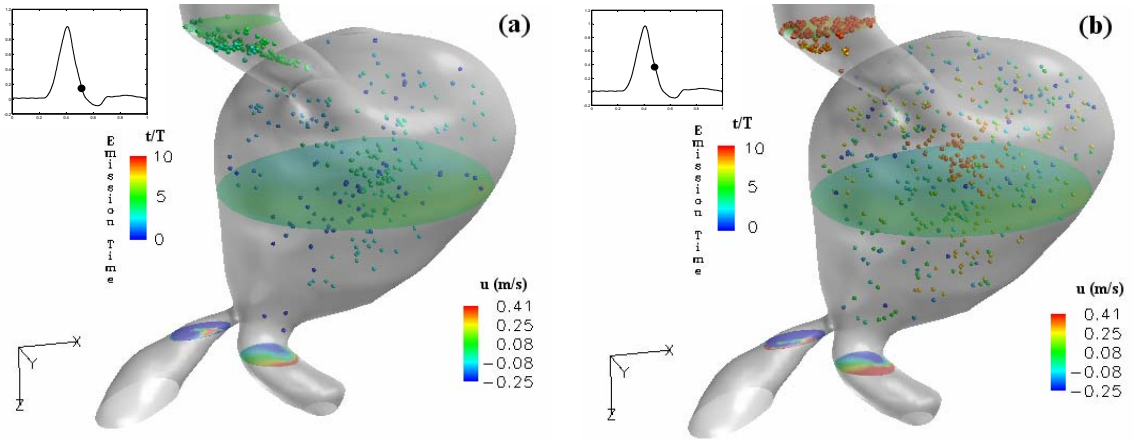

Figure 4. Snapshots of particle distribution during the systolic deceleration phase of a 10 cycle particle tracking computation after 5 cycles (a) and during the last cycle (b). Particles are color mapped with time of emission at AAA inlet. Distribution of axial component of velocity is shown on cutting planes.

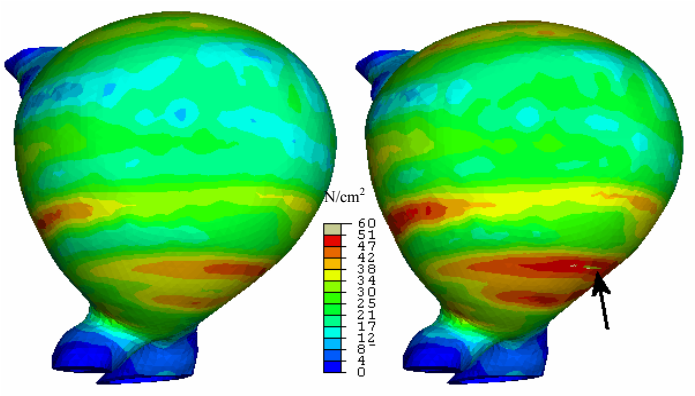

Figure 5. Computed Von Mises stress distribution on the AAA wall for uniform peak systolic pressure loading (left) and flow induced non-uniform wall loading (right). Arrow shows local maximum of wall stress.

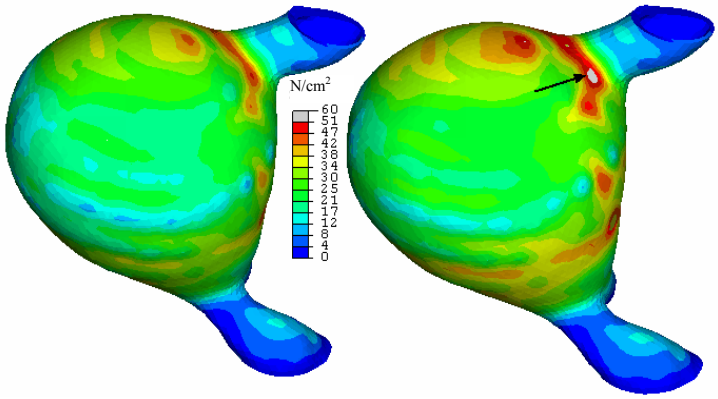

Figure 6. Computed Von Mises stress distribution on the AAA wall for uniform peak systolic pressure loading (left) and flow-induced non-uniform wall loading (right). Arrow shows local maximum of wall stress.

4 DISCUSSION

The AAA selected for this study had a peak transverse dimension of approximately 10 cm and did not rupture prior to surgery although being almost twice the size above which surgical intervention is commonly advised. This further supports the argument that the peak transverse dimension is not an absolutely reliable AAA rupture risk indicator. Model studies have shown that the law of Laplace that relates internal diameter and wall stress is not appropriate for estimating the stress field even in simplified geometry AAA's. Elger et al. [12] found in models that the wall stress distribution is most strongly influenced by the shape of the aneurysm with peak stress correlated to wall curvature.

The AAA model used in the present study includes a number of simplifications and underlying assumptions. A uniform wall thickness was specified due to the inherent limitations in the imaging technique. This affects the computed stress distribution thus increasing the uncertainty of the results as compared to the exact *in vivo* conditions. However, it does not reduce the value of the comparative results presented since it will have a similar effect in the stress distribution on both computational approaches considered. The hemodynamic pressure field was computed assuming a rigid wall model. However, it has been shown both experimentally [33] and computationally [34] that the introduction of wall compliance to arterial models only has a quantitative effect on the computed wall stresses whereas the main flow features are preserved. The computational mesh used for the structural stress analysis was based on the geometry reconstructed from the CT images obtained throughout the cardiac cycle and over multiple cycles as the acquisition was not gated to the cardiac rhythm of the subject. As a result, the mean geometric representation of the pressure pulse modulated AAA structure is reconstructed although a zero-stress state is assumed in the computation. As the zero-stress state of the AAA cannot be measured *in-vivo* one could assume that as the diastolic phase occupies most of the abdominal aorta flow cycle the reconstructed AAA geometry is an approximate representation of the diastolic pressure modulated AAA

stress state. This residual stress has been neglected in this investigation although its effects are not expected to invalidate the results of this comparative study. The effects of neglecting the residual stress on the computed stress distribution will be addressed in a future study. The material properties used in this study where based on mean values and therefore the computed stress distribution is not expected to represent the exact *in vivo* wall loading conditions. It should be noted however that the aforementioned difficulties in constructing a mathematical model to simulate *in vivo* AAA wall loading conditions also apply to the FSI approach that is even further complicated by the dynamic effects of wall motion. It is therefore very important to reduce the solution uncertainties identified in the proposed decoupled fluid structure model before introducing wall motion dynamics in a coupled fluid structure model.

Our results show that although the isolated static structural stress analysis approach captures the gross features of the stress distribution it underestimates the magnitude of the peak wall stress by as much as 12 % compared to the proposed decoupled fluid structure approach. This value may be different when other AAA cases are considered depending on the aneurysm shape and inflow conditions. However, the intra-aneurysmal flow-induced wall pressure distribution is primarily influenced by the temporal acceleration and deceleration of the flow and to a lesser extent by the size of the aneurysmal sac. Consequently, as our stress computations were based on a typical physiological AAA inflow waveform, the 12 % difference in the computed peak wall stress should be considered as a representative result. Furthermore, the decoupled fluid structure approach yields the local AAA hemodynamic conditions thus allowing for the identification of wall regions exposed to low and oscillatory wall shear stress and high shear gradients, conditions that have been linked to the development of wall lesions. This information may then be used to support prognosis of AAA rupture risk.

The significantly increased average particle residence time in the aneurysmal sac as compared to the straight tube Womersley flow solution found, highlights the association between AAA geometry, hemodynamics and thrombus formation. It has been shown *in vitro* that platelet activation, adhesion and accumulation is strongly influenced by the local hemodynamics [35]. Shear activated platelets injected in the aneurysmal sac can readily adhere and accumulate in aneurysmal wall regions exposed to low shear a process leading to thrombus formation. This process is augmented by increased platelet residence times in the vicinity of the wall that occurs when platelets are trapped in recirculation regions. Therefore detailed knowledge of the local hemodynamics may help predict sites of thrombus formation and possibly AAA growth.

In order to establish a more reliable patient specific index of AAA rupture risk it is necessary to further improve the accuracy of the computational models used. This requires imposing realistic boundary conditions extracted from the patient *in vivo* to a computational model that couples fluid and solid dynamics. This study shows that a decoupled fluid structure approach is a practical alternative to the more complete but computationally intensive FSI study.

REFERENCES

[1] Newman, A.B., Arnold, A.M., Burke, G.L., O'Leary, D.H., and Manolio, T.A. (2001), "Cardiovascular disease and mortality in older adults with small abdominal aortic aneurysms detected by ultrasonography: the cardiovascular health study", Ann Intern Med, 134, pp. 182-90.

[2] Law, M.R., Morris, J., and Wald, N.J. (1994), "Screening for abdominal aortic aneurysms", J Med Screen, 1, pp. 110-5; discussion 115-6.

[3] Sharma, U., Ghai, S., Paul, S.B., Gulati, M.S., Bahl, V.K., Rajani, M., and Mukhopadhyay, S. (2003), "Helical CT evaluation of aortic aneurysms and dissection: a pictorial essay", Clin Imaging, 27, pp. 273-80.

[4] Wolf, Y.G., and Bernstein, E.F. (1994), "A current perspective on the natural history of abdominal aortic aneurysms", Cardiovasc Surg, 2, pp. 16-22.

[5] Galland, R.B., Whiteley, M.S., and Magee, T.R. (1998), "The fate of patients undergoing surveillance of small abdominal aortic aneurysms", Eur J Vasc Endovasc Surg, 16, pp. 104-9.

[6] Participants, T.U.S.A.T. (1998), "Mortality results for randomised controlled trial of early elective surgery or ultrasonographic surveillance for small abdominal aortic aneurysms. " Lancet, 352, pp. 1649-55.

[7] Scott, R.A., Ashton, H.A., and Lamparelli, M.J. (1999), "Vascular surgical society of great britain and ireland: fifteen years of experience using 6 cm as a criterion for abdominal aortic aneurysm surgery", Br J Surg, 86, pp. 709-10.

[8] Cronenwett, J.L., Murphy, T.F., Zelenock, G.B., Whitehouse, W.M., Jr., Lindenauer, S.M., Graham, L.M., Quint, L.E., Silver, T.M., and Stanley, J.C. (1985), "Actuarial analysis of variables associated with rupture of small abdominal aortic aneurysms", Surgery, 98, pp. 472-83.

[9] Darling, R.C., Messina, C.R., Brewster, D.C., and Ottinger, L.W. (1977), "Autopsy study of unoperated abdominal aortic aneurysms. The case for early resection", Circulation, 56, pp. II161-4.

[10]Nicholls, S.C., Gardner, J.B., Meissner, M.H., and Johansen, H.K. (1998), "Rupture in small abdominal aortic aneurysms", J Vasc Surg, 28, pp. 884-8.

[11]Katz, D.A., Littenberg, B., and Cronenwett, J.L. (1992), "Management of small abdominal aortic

aneurysms. Early surgery vs watchful waiting", Jama, 268, pp. 2678-86.
[12]Elger, D.F., Blackketter, D.M., Budwig, R.S., and Johansen, K.H. (1996), "The influence of shape on the stresses in model abdominal aortic aneurysms", J Biomech Eng, 118, pp. 326-32.
[13]Mower, W.R., Baraff, L.J., and Sneyd, J. (1993), "Stress distributions in vascular aneurysms: factors affecting risk of aneurysm rupture", J Surg Res, 55, pp. 155-61.
[14]Raghavan, M.L., Vorp, D.A., Federle, M.P., Makaroun, M.S., and Webster, M.W. (2000), "Wall stress distribution on three-dimensionally reconstructed models of human abdominal aortic aneurysm", J Vasc Surg, 31, pp. 760-9.
[15]Vorp, D.A., Wang, D.H., Webster, M.W., and Federspiel, W.J. (1998), "Effect of intraluminal thrombus thickness and bulge diameter on the oxygen diffusion in abdominal aortic aneurysm", J Biomech Eng, 120, pp. 579-83.
[16]Egelhoff, C.J., Budwig, R.S., Elger, D.F., Khraishi, T.A., and Johansen, K.H. (1999), "Model studies of the flow in abdominal aortic aneurysms during resting and exercise conditions", J Biomech, 32, pp. 1319-29.
[17]Yu, S.C.M. (2000), "Steady and pulsatile flow studies in Abdominal Aortic Aneurysm models using Particle Image Velocimetry", International Journal of Heat and Fluid Flow, 21, pp. 74-83.
[18]Budwig, R., Elger, D., Hooper, H., and Slippy, J. (1993), "Steady flow in abdominal aortic aneurysm models", J Biomech Eng, 115, pp. 418-23.
[19]Taylor, T.W., and Yamaguchi, T. (1994), "Three-dimensional simulation of blood flow in an abdominal aortic aneurysm--steady and unsteady flow cases", J Biomech Eng, 116, pp. 89-97.
[20]Di Martino, E.S., Guadagni, G., Fumero A., Ballerini G., Spirito, and R., B.P., Redaelli, A. (2001), "Fluid-structure interaction within realistic three-dimensional models of the aneurysmatic aorta as a guidance to assess the risk of rapture of the aneurysm", Medical Engineering and Physics, 23, pp. 647-655.
[21]Mower, W.R., Quinones, W.J., and Gambhir, S.S. (1997), "Effect of intraluminal thrombus on abdominal aortic aneurysm wall stress", J Vasc Surg, 26, pp. 602-8.
[22]Vorp, D.A., Mandarino, W.A., Webster, M.W., and Gorcsan, J., 3rd. (1996), "Potential influence of intraluminal thrombus on abdominal aortic aneurysm as assessed by a new non-invasive method", Cardiovasc Surg, 4, pp. 732-9.
[23]Wang, D.H., Makaroun, M.S., Webster, M.W., and Vorp, D.A. (2002), "Effect of intraluminal thrombus on wall stress in patient-specific models of abdominal aortic aneurysm", J Vasc Surg, 36, pp. 598-604.
[24]Dobrin, P.B. (1989), "Pathophysiology and pathogenesis of aortic aneurysms. Current concepts", Surg Clin North Am, 69, pp. 687-703.
[25]Schurink, G.W., van Baalen, J.M., Visser, M.J., and van Bockel, J.H. (2000), "Thrombus within an aortic aneurysm does not reduce pressure on the aneurysmal wall", J Vasc Surg, 31, pp. 501-6.
[26]Raghavan, M.L., and Vorp, D.A. (2000), "Toward a biomechanical tool to evaluate rupture potential of abdominal aortic aneurysm: identification of a finite strain constitutive model and evaluation of its applicability", J Biomech, 33, pp. 475-82.
[27]Di Martino, E., Mantero, S., Inzoli, F., Melissano, G., Astore, D., Chiesa, R., and Fumero, R. (1998), "Biomechanics of abdominal aortic aneurysm in the presence of endoluminal thrombus: experimental characterisation and structural static computational analysis", Eur J Vasc Endovasc Surg, 15, pp. 290-9.
[28]Wang, D.H., Makaroun, M., Webster, M.W., and Vorp, D.A. (2001), "Mechanical properties and microstructure of intraluminal thrombus from abdominal aortic aneurysm", J Biomech Eng, 123, pp. 536-9.
[29]Finol, E.A., Di Martino E.S., Vorp, D.A., Amon, C.H. (2003), "Fluid-structure interaction and structural analyses of an aneurysm model", *Proceedings of the Summer Bioengineering Conference*, Key Biscane, Florida, pp. 75-76.
[30]Giordana, S., Sherwin, S.J., Peiro, J., Doorly, D.J., Papaharilaou, Y., Caro, C.G., Watkins, N., Cheshire, N., Jackson, M., Bicknall, C., and Zervas, V. (2005), "Automated classification of peripheral distal by-pass geometries reconstructed from medical data", J Biomech, 38, pp. 47-62.
[31]Perktold, K., Resch, M., and Florian, H. (1991), "Pulsatile non-Newtonian flow characteristics in a three-dimensional human carotid bifurcation model", J Biomech Eng, 113, pp. 464-75.
[32]Womersley, J.R. (1955), "Method for the calculation of velocity, rate of flow and viscous drag in arteries when the pressure gradient is known", J Physiol, 127, pp. 553-63.
[33]Duncan, D.D., Bargeron, C.B., Borchardt, S.E., Deters, O.J., Gearhart, S.A., Mark, F.F., and Friedman, M.H. (1990), "The effect of compliance on wall shear in casts of a human aortic bifurcation", J Biomech Eng, 112, pp. 183-8.
[34]Perktold, K., and Rappitsch, G. (1995), "Computer simulation of local blood flow and vessel mechanics in a compliant carotid artery bifurcation model", J Biomech, 28, pp. 845-56.
[35]Karino, T., and Goldsmith, H.L. (1984), "Role of blood cell-wall interactions in thrombogenesis and atherogenesis: a microrheological study", Biorheology, 21, pp. 587-601.